JTTEE5 15:356-363
DOI: 10.1361/105996306X124356
1059-9630/$19.00 © ASM International

Peer Reviewed

Dense Si_3N_4 Coatings with High Friction Coefficient Deposited by High-Velocity Pulsed Plasma Spraying

S. Usuba and R.B. Heimann

(Submitted September 4, 2005; in revised form December 10, 2005)

A novel electromagnetically accelerated plasma spraying technique was applied to mixtures of αSi_3N_4, and alumina, yttria, and silica additives to deposit thin coatings (50-100 μm) onto mirror-polished stainless steel surfaces. The dense coatings consisted of crystalline αSi_3N_4 with minor amounts of β′SiAlON, traces of βSi_3N_4 and $Y_3Al_5O_{12}$ as well as a quinary Si-Al-N-O-Y glass. The adhesion strengths depended on the powder particle size showing values of >77 MPa for coarse powders (median grain size 25 μm) and >67 MPa for fine powders (median grain size 8 μm). The average indentation hardnesses were 450 $HV_{0.025}$ (coarse powder) and 620 $HV_{0.025}$ (fine powder); the sliding wear resistances were comparable to those of sintered Si_3N_4 used as counterbody in a pin-on-disc friction test. The friction coefficient showed surprisingly large values (1.0-1.1 in water and 1.3-1.4 in air), suggesting application of such coatings as tribological high-friction surfaces.

Keywords electromagnetically accelerated plasma spraying, friction coefficient, hardness, microstructure, silicon nitride coatings, sliding wear

1. Introduction

Silicon nitride ceramics show excellent mechanical properties (i.e., high bending strength, elastic modulus and fracture toughness up to 1400 °C, high abrasion wear and solid particle erosion resistance, and low density), thermal properties (i.e., low coefficient of thermal expansion and high thermoshock resistance), and chemical properties (i.e., stability against most acids and bases, corrosive gases, and liquid metals) that are being exploited in diverse technologically challenging fields (Ref 1, 2). These include but are not limited to applications as roller and ball bearings, coil and disc spring material, cutting tools for high-speed machining of hard steels and superalloys, heat exchangers and heat pumps, inert gas welding and brazing fixtures and pins, stationary blades and burner nozzles of gas turbines, moulds for pressure casting of light metals, and ladles and tundishes for horizontal casting of steel tubes (Ref 3). Particularly promising areas of application exist in gasoline and diesel engines, including exhaust valves, valve spring retainers, bucket tappets, rocker arm pads, pistons of internal combustion engines, and turbocharger rotors (Ref 4). However, major barriers to the incorporation of these parts into standard power trains and engines of passenger cars relate to the cost of processing, and the severe technological problem of mass-producing complex ceramic components with a very high degree of reproducibility and long-term reliability. Hence, in many cases the use of monolithic ceramic parts poses problems both during manufacturing and in service. For example, experimental turbocharger rotors and pistons of internal combustion engines are still prone to failure in service owing to their inherently brittle nature. If these parts could be made from tough, high-temperature-resistant metals that provide superior mechanical stability and in turn are being protected against the attack of highly corrosive combustion gases by a mechanically, thermally, and chemically compatible silicon nitride coating, then a longer service life as well as increased combustion temperature, and hence environmentally beneficial engine performance, could be expected.

Deposition of pure silicon nitride coatings by conventional thermal spraying has been considered to be impossible because Si_3N_4 dissociates and in turn sublimates above 1800 °C. It is also subject to oxidation in the presence of an oxygen-containing atmosphere at elevated temperatures. Thin amorphous silicon nitride films are frequently deposited by chemical vapor deposition and applied as masking layers for semiconductor integrated circuits during profile etching, diffusion barriers in very large scale integration (VLSI) production lines, for damage protection of optical fibers, as gate dielectrics for specific metal insulator semiconductor memory devices (Ref 2), and as moisture barrier for organic light-emitting diode (OLED) displays (Ref 5). However, attempts to deposit mechanically stable thick silicon nitride coatings by thermal spraying using metallic (Ref 6–8) or silicate glass binders (Ref 9), conversion in the as-deposited state through a reactive spray process (Ref 10), or in situ nitridation in flight (Ref 11) were not met with resounding success as such coatings contain only little silicon nitride but rather substantial amounts of embrittling metal silicides. More successful were endeavors to prepare high-Si_3N_4 coatings starting from $\beta' Si_{6-z}Al_zO_zN_{8-z}$ powders with different degrees of substitution, z (Ref 12) or clad-type powder consolidation using alloy bond coats (Ref 13). Recently, it was recognized that high particle velocities generated by detonation spraying, Top Gun technology, high-frequency pulse detonation, and accelerated plasma

S. Usuba, National Institute for Advanced Industrial Science and Technology (AIST), Tsukuba, Ibaraki, Japan; and **R.B. Heimann,** Department of Mineralogy, Technische Universität Bergakademie Freiberg, Freiberg, Germany. Contact e-mail: robert.heimann@ocean-gate.de.

spraying with axial powder injection were conducive to depositing dense and well-adhering silicon nitride coatings (Ref 14–18). In addition, the optimization of heat transfer into the powder particles was found to be one of the most decisive factors (Ref 18). This necessitates special powder preparation procedures (Ref 19, 20).

To continue research along this line of reasoning in this article, extremely high powder particle velocities up to 3 km/s, which were generated by an electromagnetically accelerated plasma (EMAP), were exploited to deposit dense, homogeneous silicon nitride coatings with desirable mechanical properties that adhere well to polished steel surfaces.

2. Materials and Experimental Methods

2.1 Powder Preparation

The powders used for EMAP spraying (EMAPS) were synthesized by mixing αSi_3N_4 powder (Silzot 7038; SKW Trostberg, Germany) with sintering aids such as alumina, yttria, silica, and AlN, agglomerating by spray drying using an organic binder, and subsequent sintering at 1450 °C in a nitrogen-containing atmosphere (Ref 18-20). After sintering, the powders were mechanically treated by a mild milling process and finally fractionated by dry sieving. Three types of powder composition were tested: 68 mass% Si_3N_4 + 16 mass% Al_2O_3 + 16 mass% Y_2O_3 (powder 1; OBSN 3 [Ref 16]); 65 mass% Si_3N_4 + 11 mass% Al_2O_3 + 12 mass% Y_2O_3 + 4 mass% AlN, + 8 mass% SiO_2 (powder 2; OBSN 13 [Ref 16]); and the as-received powder 1 that was ball-milled for 2 h to reduce its grain size (powder 3). The addition of SiO_2 decreases the viscosity of the alumina-yttria binder matrix during sintering, while the addition of AlN promotes the formation of SiAlON. The grain size fraction −45 + 20 μm was used for EMAPS of powders 1 and 2.

2.2 Experimental Method

The operating principle of EMAPS is shown in Fig. 1 (Ref 21). The spraying system consists of an evacuated accelerating channel that comprises a pair of parallel electrodes connected to a high-current power source by a switch, and a vessel that contains a pressurized gas and the powder source. The process is being initiated by activating a fast-opening valve at the nozzle of the vessel (Fig. 1a). After introducing the powder and the working gas into the accelerating channel (Fig. 1b), an arc discharge is initiated at the desired position in the accelerating channel, while the powder remains suspended in the accelerating channel (Fig. 1c). The plasma at the arc-initiating point then receives an electromagnetic force (Lorentz force) and forms an EMAP of the working gas that heats and propels the powder toward the substrate (Fig. 1d and e).

Figure 2 shows a schematic diagram of the apparatus consisting of a coaxial cylindrical accelerating channel (outer and inner diameters 70 and 40 mm, respectively; effective length 360 mm) equipped with powder and working gas feeders, an arc igniter, and a capacitor bank (Nichicon, Kyoto, Japan; 3 mF). The typical discharge pulse of the capacitor bank peaks at about 100 kA and lasts about 300 μs. The accelerating channel and the substrate chamber will be evacuated to a pressure of <0.1 kPa.

The amount of the powder used per single shot is typically

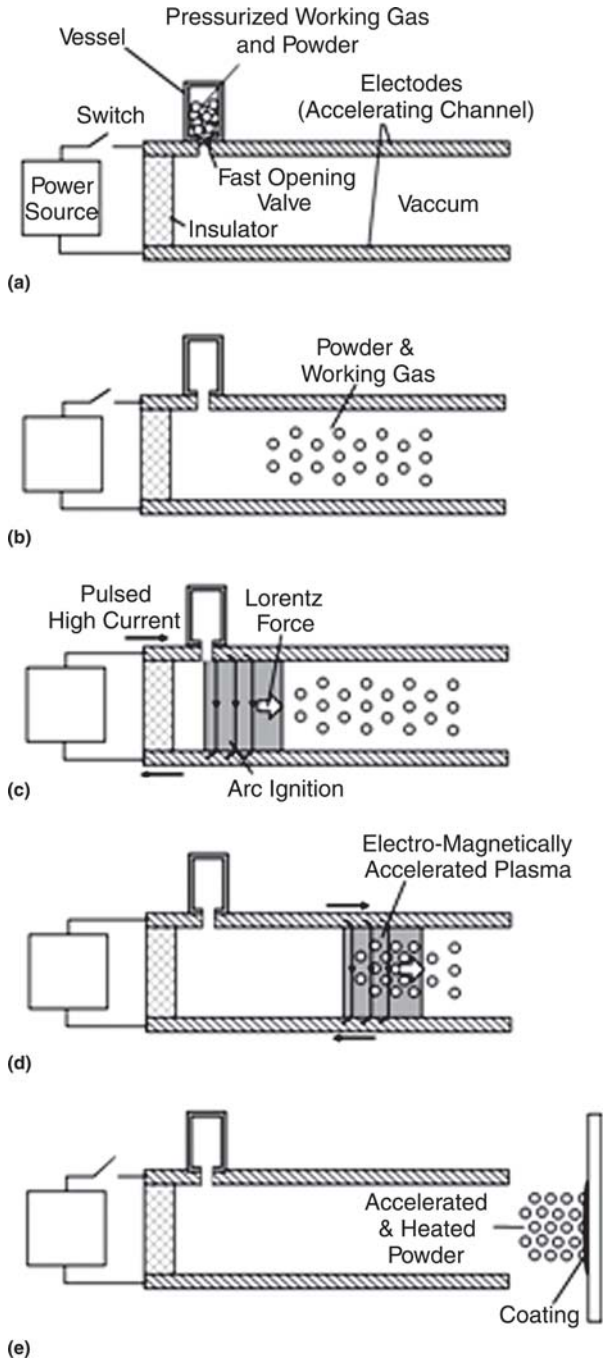

Fig. 1 Operational principle of EMAPS

0.1 g. The powder container with a volume of 15 cm^3, which is typically pressurized with 8 MPa argon, is initially closed by a polymer diaphragm playing the role of a fast-opening valve. At a given time, the electric explosion of a metallic lead wire located near the diaphragm causes the instantaneous rupture of the diaphragm and the subsequent injection of the powder into the evacuated accelerating channel. To initiate a high-current arc discharge at the desired position in the accelerating channel, an electric spark is used to establish an instantaneous electrical bridging between the inner and outer electrodes.

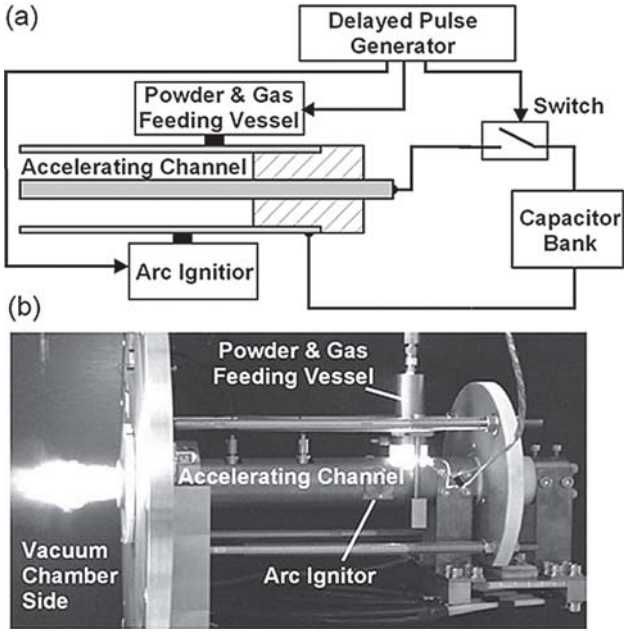

Fig. 2 (a) Schematic diagram of the experimental setup, and (b) appearance of the plasma generation in air

The Si_3N_4 powders were deposited onto mirror-polished stainless steel (S.S.) coupons (SUS304) that were 15 × 15 × 2 mm in size and were positioned 50 mm from the plasma exit nozzle of the apparatus. Because the deposition rate was only 1 to 2 μm per single spraying shot, the formation of a coating of 50 to 100 μm thickness required 40 to 50 iterative spray cycles, which necessitated the replacement of the diaphragm after each shot.

Figure 3 shows the calculated final particle velocity (a) and the particle dwell time (b) as functions of the particle diameter and the apparent density, based on a simplified plasma model in which the EMAP was treated as a fast-traveling uniform gas with a limited column length. A traveling velocity of 2.5 km/s and a length of the gas column of 120 mm were assumed to exist based on experimental observations (Ref 22); a gas temperature of 10,000 K was estimated from the shock-compressed state of the working gas the pressure of which is balanced by a maximum electromagnetic pressure of about 0.9 MPa. Details of the model will be presented elsewhere. The calculated values of the final particle velocity shown in Fig. 3 are in approximate agreement with experimental observations (Ref 22). In the present contribution, this model was used to estimate the differences in spraying conditions among the three types of powder.

2.3 Characterization of Powders and Coatings

The starting powders and the coatings deposited were examined using an x-ray diffractometer (RINT2500; Rigaku, Tokyo, Japan), and a high-resolution scanning electron microscope (HR-SEM) (S-5000; Hitachi, Tokyo, Japan). For the HR-SEM observations a 10 nm, Pt-Pd layer was deposited onto the samples. The microstructure of the deposited material was examined by transmission electron microscopy (TEM) (model EM-922; Leo, Oberkochen, Germany). The samples for the TEM measurement were prepared by simply crushing the coating material separated from the substrate.

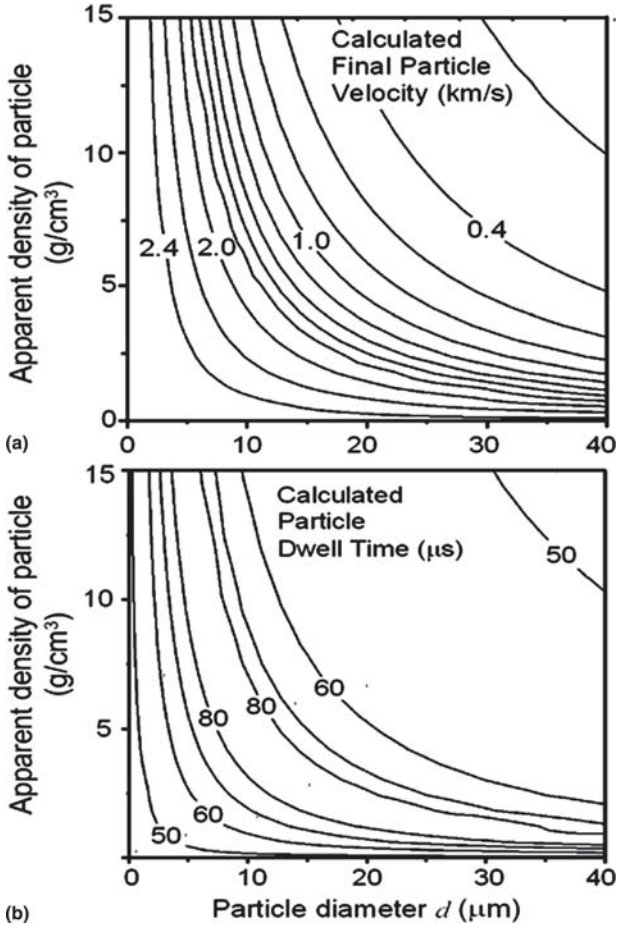

Fig. 3 (a) Calculated final particle velocity and (b) dwell time as functions of the apparent density and the diameter of the particles

Micro-Vickers indentation hardness measurements (DHM-2; Matsuzawa Seiki, Tokyo, Japan) with an indenting load of 25 g were carried out on cross sections of resin-embedded particles of starting powders 1 and 2 as well as on polished cross sections of the coatings. For each sample, measurements were performed at 20 different positions, and the HV value calculated at a 95% confidence level using a t-distribution. The adhesion strengths of the coatings were measured according to ISO14916 designation using SUS304 substrate fixtures of 25 mm diameter and 28 mm length. Coatings produced from powders 1 and 3 were deposited onto the mirror-polished surfaces of the fixtures that subsequently were glued with epoxy resin to the corresponding loading fixtures. The friction coefficients between as-sprayed coatings and sintered Si_3N_4 balls were measured by a pin-on-disc friction tester (Takachiho Seiki, Tokyo, Japan) with a load of 1 N and a sliding speed of 10 mm/s for 1 h in distilled water and air.

3. Results and Discussion

3.1 Composition of Powders

Figure 4 shows the grain size distribution of powders 1 and 3. The median grain size of powder 1 (~25 μm) was reduced by

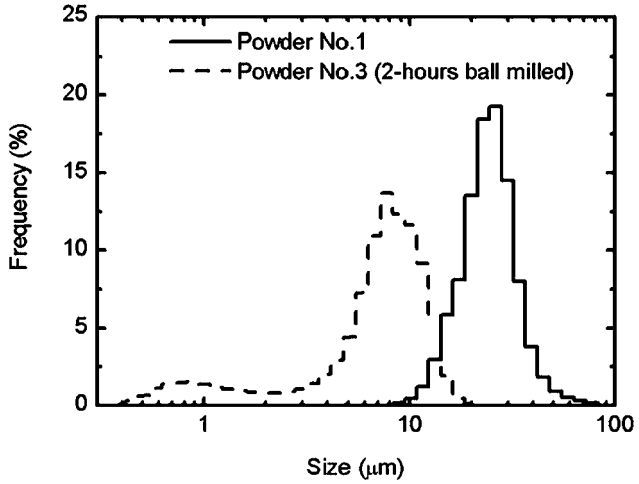

Fig. 4 Size distributions of powders 1 and 3

ball-milling to ~8 μm (powder 3). Figure 5(a) shows a SEM of powder 1 consisting of "raspberry-shaped" spherical, porous particles with a central hole formed by the evaporation of the organic binder and water during spray drying. The open porosity was determined to be ~30%, and the density of the pore-free product to be 3.41 Mg/m^3 (Ref 18). No apparent pores were observed in cross sections of the particles of powder 2 using light optical microscopy.

The x-ray diffraction (XRD) pattern of the powders (Fig. 6) revealed the existence of four phases: αSi_3N_4; βSi_3N_4; β'SiAlON; and $Y_3Al_5O_{12}$ (YAG). The latter phase is indicated by a solid dot in Fig. 6. During sintering, the starting αSi_3N_4 transforms gradually to metastable βSi_3N_4. The reaction of silicon nitride with the oxides of the binder phase at high temperature can be described schematically as

$$\beta\text{-}Si_3N_4 + Al_2O_3 + Y_2O_3 + SiO_2 \rightarrow \beta'\text{-}Si_{6-z}Al_zN_{8-z} + \text{Y-Si-Al-O-N glass(I)} \quad \text{(Eq 1)}$$

Slow cooling leads to the partial devitrification of glass (I) to form crystalline YAG and glass (II). For example, for $z = 1$ this reaction can be expressed by Eq 2:

$$Si_5AlON_7 + \text{glass(I)} \rightarrow Si_{5+x}Al_{1-x}O_{1-x}N_{7+x} + Y_3Al_5O_{12} + \text{glass(II)} \quad \text{(Eq 2)}$$

The amount of YAG in powders 1 and 3 is considerably higher than in powder 2, owing to the higher concentration of alumina and yttria in the former. The solid solution of Al_2O_3 in βSi_3N_4 to form β'SiAlON is accompanied by the expansion of the unit cell. Hence, the degree of substitution z of, respectively, Si by Al, and N by O can be estimated considering the change of the lattice parameters a_0 and c_0 of the hexagonal βSi_3N_4 structure according to the equations $a = a_0 + 0.002967 \cdot z$ and $c = c_0 + 0.002554 \cdot z$ (Ref 23), whereby $a_0 = 0.7603$ nm and $c_0 = 0.2907$ nm denote the lattice constants of pure βSi_3N_4. This leads to $z = 1.4$ for powders 1 and 3, and $z = 1.9$ for powder 2.

Table 1 summarizes the physical properties of the powders

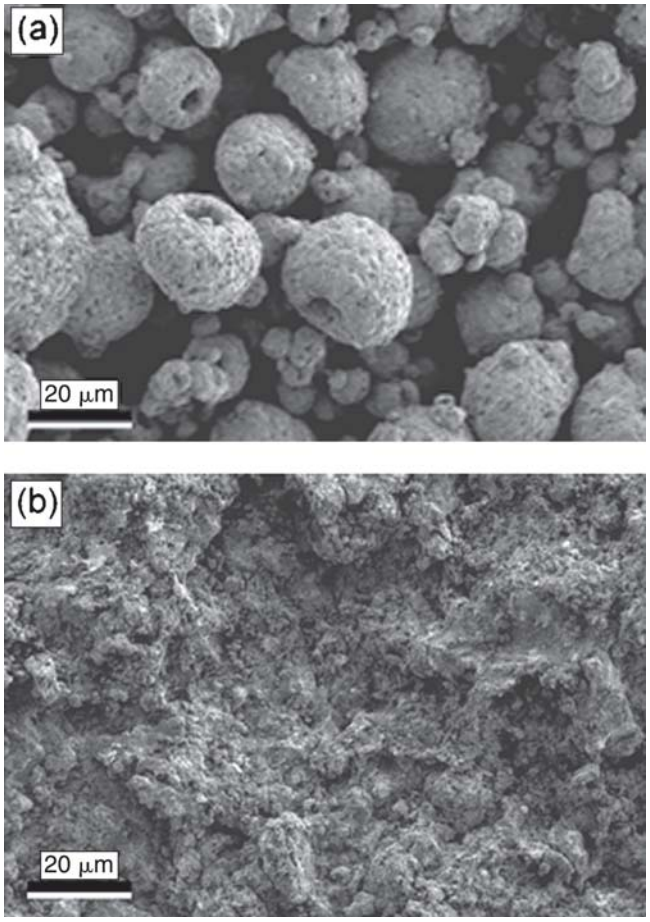

Fig. 5 SEM micrographs of (a) powder 1 and (b) the surface of a coating produced from powder 1

and the estimated spray conditions. It is obvious that powder 2 consists of considerably harder and denser particles compared with powder 1. The hardness of powder 3 was expected to be equivalent to that of powder 1. Spray conditions estimated from Fig. 3 show that the differences in particle size and apparent density resulted in notable differences in the particle velocities but did not affect dwell times.

3.2 Composition of Coatings

The XRD patterns shown in Fig. 6 indicate that the coatings consist of αSi_3N_4 (open circles) and minor amounts of βSi_3N_4 (dash), β'SiAlON ("T"), and YAG (solid circles). Evidently, the crystalline YAG of the precursor powders 1 and 3 redissolved in the glass, the existence of which is indicated by the elevated background of the XRD pattern between 25 and 40 $^o2\theta$, as shown in Fig. 6(a) and (c). These findings are in accord with results obtained earlier by detonation gun spraying of powders of identical composition (Ref 18). In coatings produced from powder 2, no significant compositional changes were observed. The Fe observed in powder 3 (Fig. 6c) likely originated from the steel balls used in the milling process. It should be noted that in the XRD pattern of the coating from powder 3, a broad hump centered at 17 $^o2\theta$ as well as a distinct peak at 21.4 $^o2\theta$, possibly

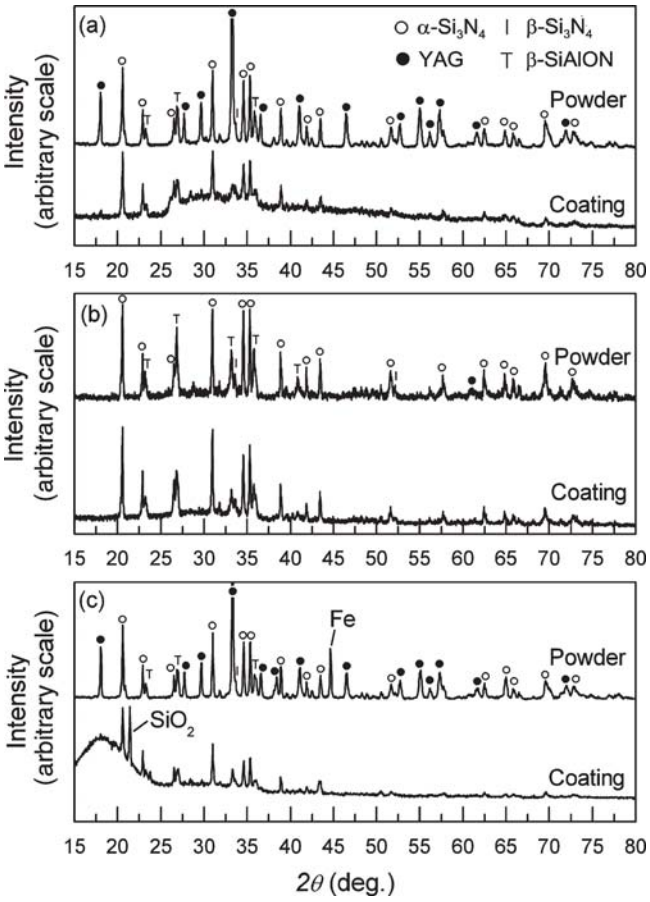

Fig. 6 The XRD pattern of powders and coatings: (a) powder 1; (b) powder 2; and (c) powder 3

related to SiO_2, appeared, whereas the Fe peak had disappeared. The broad hump suggests a significant increase in a glass phase with silica content higher than that observed in the coating from powder 1. The maximum temperature of particles of powder 3 in the plasma is expected to be significantly higher than that of powder 1, owing to their much smaller size compared with that of powder 1 but showing identical dwell time. Furthermore, the high spraying velocity of powder 3 is expected to result in a high degree of deformation and subsequently in a high cooling rate. Such intense heating and rapid cooling processes of the particles in powder 3 are a possible explanation for the increase in the amount of glass phase in which Fe was presumably dissolved. The appearance of SiO_2 also suggests a different heating history of powder 3 compared with powder 1, although the mechanism of SiO_2 formation is not yet clear.

3.3 Microstructure of Coatings

Figure 5(b) shows the surface of a coating that was produced with powder 1, which attests to the heavy deformation that the original porous powder grains (Fig. 5a) underwent during their impact of the substrate surface with supersonic velocity.

The thickness of the coatings after 50 iterative sprayings varied between 50 and 100 μm, owing to a waviness of the coating surface of as yet unknown origin. Figure 7 shows cross sections

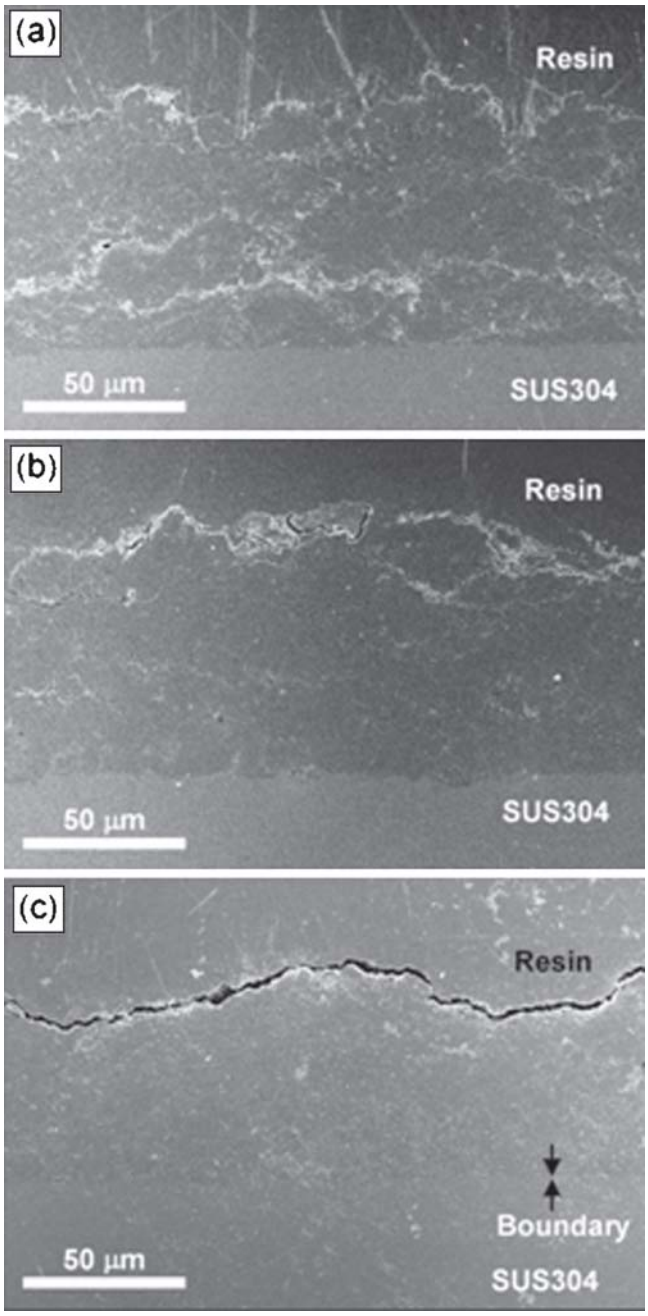

Fig. 7 SEM micrographs of cross sections of coatings from powders 1(a), 2 (b), and 3 (c)

of the coatings. The coatings from powders 1 and 2 are generally dense, but some pores and microcracks are visible. The coating from powder 3 is dense without apparent pores or cracks. The interface S.S. substrate/coating is remarkably smooth and continuous, suggesting excellent coating adhesion (see section 3.5). Some coating material was found to be embedded into the mirror-polished S.S. substrate, which was evidently caused by the high-velocity impact of solid particles at the substrate surface. This mechanism may be akin to explosive cladding. On impact with supersonic velocity, a solid or only partially molten particle will generate a shock wave propagating into the substrate. The

Table 1 Physical properties of the powders and estimated spray conditions

Powder	Particle size(a), μm	Apparent density of particles(b), Mg/m^3	Vickers hardness, $HV_{0.025}$	Spray conditions(c)	
				Particle velocity, km/s	Dwell time, μs
1	25	2.4	310 ± 120	1.4	70
2	25	3.4	1070 ± 160	1.0	65
3	8	2.4	…(d)	2.3	70

(a) Median size obtained by laser diffraction measurements. (b) Assuming porosity 0% for powder 2, 30% for powders 1 and 3, and a pore-free density of 3.41 Mg/m^3 for all powders. (c) Estimated from Fig. 3. (d) Not measured because of insufficient cross-sectional area

porosity of the particle takes on a particular significance as its P-V adiabat (Rankine-Hugoniot equation of state) lies above that of dense material, owing to an increase in thermal energy as the result of the compression of the porous material. This also causes an increase in the thermal pressure component. Because the shock wave gives rise to multiple collisions between crystal grains within the porous particle, very strong local pressures are being generated, causing additional compression, heating, and crushing of the particle (Ref 24, 25). This strong crushing effect is manifest in the appearance of the coating surface (Fig. 5b).

The TEM studies were conducted on a crushed coating sample from powder 3, which is the only sample that included sufficiently thin particles. Figure 8 shows a typical TEM micrograph of such a crushed sample indicating the existence of crystalline particles (arrows 1–3) in an amorphous matrix (Ref 4). The high-resolution TEM (HR-TEM) lattice fringes of particles 1 and 2 reveal an interplanar spacing value of approximately 0.67 nm that can be assigned to the (100) spacing of βSi_3N_4 (or β′SiAlON). This micrograph indicates that the typical size of βSi_3N_4 or β′SiAlON particles is ~20 nm, at least in the coating generated from powder 3.

3.4 Mechanical Properties of Coatings

Table 2 summarizes the results of the Vickers indentation hardness measurements of the coatings. These hardness values are equivalent to those observed earlier on detonation gun-sprayed Si_3N_4-based coatings produced with powder 1 (Ref 18). However, it should be emphasized that the determination of the indentation microhardness of thermally sprayed coatings and the interpretation of the results are problematic, owing to the generally heterogeneous microstructure of such coatings as well as the presence of large amounts of glassy phase. Moreover, the influence of the substrate must be considered, which renders the measured "composite" microhardness, a very complex function of the mechanical properties of both the coating and the substrate (e.g., Ref 26). Hence, it is thought that measuring the wear resistance of a coating reflects the desired technological performance much better (Ref 18) (see section 3.5).

The hardness of coatings from powders 1 and 3 is higher than those of the starting powders. Such hardening, together with the dense cross section of the coatings shown in Fig. 7(a) and (c), attests to a substantial densification of the initially porous particles during the deposition process. It should be noted that the coating of powder 2, consisting of dense and hard particles, does not show a higher hardness than the coating from powder 3. This suggests the importance of a compliant glassy phase, promoting interparticle bonding, for the hardness development of the coating. The formation of the glass phase is considered to be influenced not only by the powder composition but also by the apparent powder density and size that connect to the spray velocity, and by the temperature rise in the plasma. The proper selection of these parameters will be essential in controlling the quality of Si_3N_4-based coatings.

Table 2 Mechanical properties of the coatings

Coating/powder	Vickers hardness, $HV_{0.025}$		Adhesion strength, MPa
	Powders	Coatings	
1	310 ± 120	450 ± 117	>76.6(a)
2	1070 ± 160	542 ± 119	…
3	…	620 ± 101	>67.5(a)

(a) Exceeding the tensile stress at which internal failure of the epoxy resin occurred

Table 2 also shows the results of adhesion strength measurements of the coatings from powders 1 and 3. During tensile testing, failure always occurred in the layer of the epoxy resin adhesive. The adhesion strengths of coatings from powders 1 and 3 were thus determined to exceed 76.6 and 67.5 MPa, respectively.

3.5 Friction and Sliding Properties

The friction coefficient between a polished Si_3N_4 ball and a polished sintered monolithic Si_3N_4 slab was reported to be <0.1 in water under specific sliding conditions (Ref 27). Considering the influence of the sliding speed (Ref 27) and the initial surface roughness (Ref 28), the friction coefficient attained under the conditions prevailing in this work was expected to approach values between 0.6 and 0.7. However, as shown in Fig. 9, the friction tests involving a sintered Si_3N_4 ball and EMAPS silicon nitride coatings showed surprisingly rather steady and significantly higher friction coefficient values of 1.0 to 1.1 in water, and even higher values of 1.3 to 1.4 in air. After being scratched by the Si_3N_4 ball during the friction test, all coatings remained tightly attached to the S.S. substrate except for minor localized chipping that resulted in the exposure of the S.S. substrate surface (Fig. 10a). Correspondingly, the surface of the sliding ball showed significant wear by grooving, indicating that at least some parts of the coatings had a hardness and wear resistance that were comparable to or even exceeded those of the sintered Si_3N_4 ball (Fig. 10b). The almost identical friction and wear properties of coatings produced from powders 1 and 2 suggest that there was no significant difference in hardness and adhesion

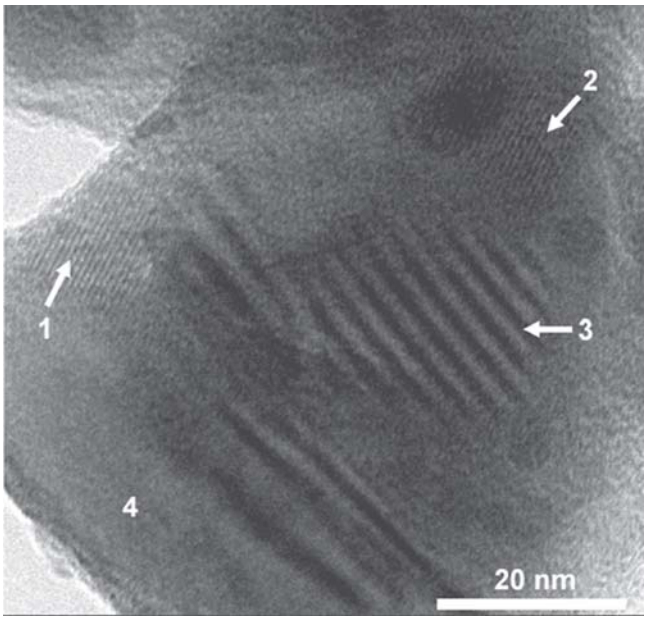

Fig. 8 TEM micrograph of coating material from powder 3 showing crystalline nanoparticles (1-3) in an amorphous matrix (4). The distance of the HR-TEM lattice fringes of particles 1 and 2 is ~0.67 nm.

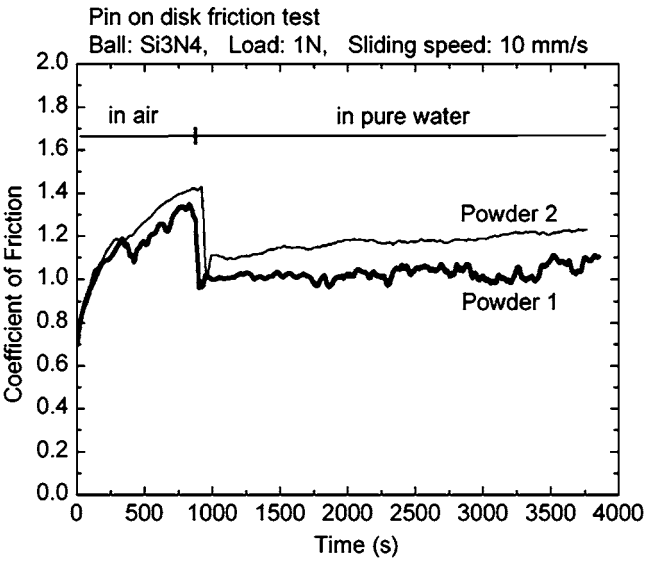

Fig. 9 Friction coefficients of coatings from powders 1 and 2 in air and water

strength of the two types of coating, at least not under the conditions of the friction tests performed.

4. Conclusions

The Si_3N_4 coatings deposited by EMAPS onto S.S. surfaces show excellent adhesion, high abrasion, and sliding wear resistance, and extremely high friction coefficients in air and water

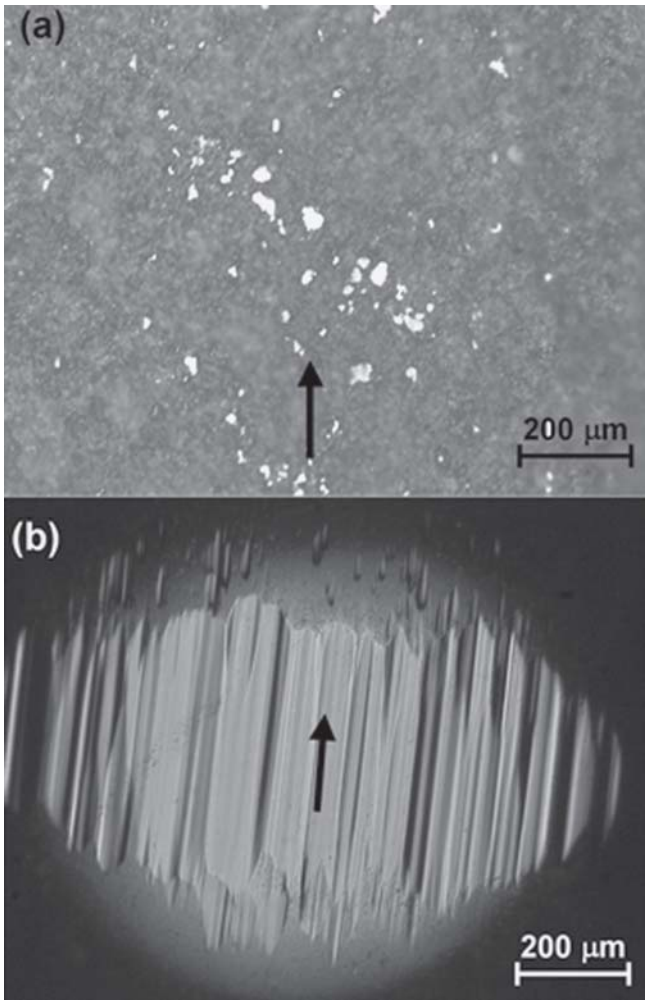

Fig. 10 Light optical micrographs of the wear surfaces of a coating from powder 1 (a) and the Si_3N_4 ball (b). The arrow indicates the direction of slide.

exceeding values of 1.0. Such coatings could be used to provide tribological surfaces for automotive brake pads actuating against gray cast iron rotors (Ref 29), improved grip-and-release surfaces for printing rolls, or high friction coatings between sliding interfaces to damp the vibrations of positioning equipment operating in outer space. Likewise, silicon nitride coatings could be applied to protect the internal surfaces of tool steel pressure-casting moulds from chemical attack by molten light metals and their alloys, and thus to provide a semipermanent release interface. The excellent coating performance notwithstanding, the batch-type mode of EMAPS with the required replacement of the powder and gas feeding vessel after each shot renders the novel deposition technique uneconomical at present. Hence, scale-up and optimization work have to be carried out during future development cycles.

Acknowledgments

The authors are indebted to Dr. L.-M. Berger, the Institute of Materials and Beam Technology, of the Fraunhofer Society

(Dresden, Germany), for providing the spray powders, to Dr. S. Sodeoka, AIST (Tsukuba, Japan), for adhesion strength testing, and to Dr. K. Yamamoto of the same institution for the TEM micrographs.

References

1. L. Michalowsky, Ed., *New Ceramic Materials*, Deutscher Verlag für Grundstoffindustrie, Leipzig, Stuttgart, Germany, 1994, in German
2. F.L. Riley, Application of Silicon Nitride Ceramics, *Advanced Ceramic Materials*, *Key Engineering Materials,* H. Mostaghaci, Ed.,Trans Tech Publ. Ltd., Zurich, Switzerland, 1996, 122/124, p 479-488
3. R.B. Heimann, S. Thiele, B. Wielage, M. Zschunke, M. Herrmann, and L.-M. Berger, Entwicklung von Schichten auf Siliziumnitrid-Basis als HT-erosionsbeständiger Werkstoff für thermische Anlagen, *Freiberger Forschungshefte (Maschinenbau),* W. Schuik, G. Walter, Ed., 1997, A848, p 166-182, in German
4. K.D. Mörgenthaler and H. Bühl, Ceramics for Engines, *Tailoring of Mechanical Properties of Ceramics,* M. J. Hoffmann, G. Petzow, Ed., NATO ASI Series E. Applied Sciences, Kluwer, Dordrecht, The Netherlands, 1994, p 429-441
5. D.S. Wu, W.C. Lo, C. Chiang, H.B. Lin, L.S. Chang, R.H. Horng, C.L. Huang, and Y.J. Gao, Water and Oxygen Permeation of Silicon Nitride Films Prepared by Plasma-enhanced Chemical Vapor Deposition, *Surf. Coat. Technol.,* 2005, **198,** p 114-117
6. E. Lugscheider and R. Limbach, Plasma Spraying of Agglomerated Powders on the Basis of Si_3N_4, *DVS Berichte,* 130, Deutscher Verlag für Schweisstechnik, Düsseldorf, Germany, 1990, p 224-225, in German
7. E. Lugscheider, R. Limbach, A. Liden, and J. Lodin, Plasma Spraying of Silicon Nitride (Si_3N_4), in *Proc. Conf. High Temp. Mater. Powder Eng.,* Liege, Belgium, 1, F. Bachelet, Ed., Kluwer, Dordrecht, The Netherlands, 1990, p 877-880
8. R. Limbach, Development of Thermally Sprayed Wear Resistant Coatings with Favorable Tribological Behavior, *Techn.-Wiss. Berichte Lehr- und Forschungsgebiet Werkstoffwissenschaften der RWTH Aachen,* Nr. 37.03.12.92, E. Lugscheider, Ed., 1992, in German
9. A. Kucuk, R.S. Lima, and C.C. Berndt, Composite Coatings of Si_3N_4-Soda Lime Silicate Produced by the Thermal Spray Process, *J. Mater. Eng. Perform.,* 2000, **9,** p 603-608
10. T. Eckardt, W. Malléner, and D. Stöver, Reactive Plasma Spraying of Silicon in Controlled Nitrogen Atmosphere, *Thermal Spray Industrial Applications,* C.C. Berndt and S. Sampath, Ed., June 20-24, 1994 (Boston, MA), ASM International, 1994, p 515-519
11. T. Eckardt, W. Malléner, and D. Stöver, Development of Plasma Sprayed Silicon/Silicon Nitride Coatings by In-Situ Nitridation, *Thermische Spritzkonferenz: TS96,* E. Lugscheider, Ed., DVS Berichte, 175, Deutscher Verlag für Schweisstechnik, Düsseldorf, Germany, 1996, p 309-312, in German
12. S. Sodeoka, K. Ueno, Y. Hagiwara, and S. Kose, Structure and Properties of Plasma-Spayed SiAlON Coatings, *J. Therm. Spray Technol.,* 1992, **1,** p 153-159
13. T. Tomota, N. Miyamoto, and H. Koyama, Formation of Thermal Spraying Ceramic Layer, Patent JP 63 169371, A. Int. Cl.[4]: C23C 4/10, Filing date 29.12.1986, Publication date July 13, 1988, Patent Abstracts of Japan, 1988, **12**(446), 24.11.1988, in Japanese
14. S. Thiele, R.B. Heimann, M. Herrmann, L.-M. Berger, M. Nebelung, M. Zschunke, and B. Wielage, Thermal Spraying of Silicon Nitride-Based Powders, *Thermal Spray: Practical Solutions for Engineering Problems,* C.C. Berndt, Ed., Oct 7–11, 1996 (Cincinnati, OH), ASM International, 1996, p 325–331
15. L.-M. Berger, M. Herrmann, M. Nebelung, S. Thiele, R.B. Heimann, T. Schnick, B. Wielage, and P. Vuoristo, Investigations on Thermal Spraying of Silicon Nitride-Based Powders, *Thermal Spray: Meeting the Challenges of the 21st Century,* C. Coddet, Ed., May 25-29, 1998 (Nice, France), ASM International, 1998, p 1149-1154
16. R.B. Heimann, S. Thiele, L.-M. Berger, M. Herrmann, M. Nebelung, B. Wielage, T.M. Schnick, and P. Vuoristo, Thermally Sprayed Silicon Nitride-Based Coatings on Steel for Application in Severe Operation Environments: Preliminary Results, *Microstructural Science: Analysis of In-Service Failures and Advances in Microstructural Characterization, 26,* E. Abramovici, D.O. Northwood, M.T. Shehata, and J. Wylie, Ed., ASM International, 1998, p 389-394
17. R.B. Heimann, S. Thiele, L.-M. Berger, M. Herrmann, and P. Vuoristo, Detonation Spraying of Silicon Nitride for High Temperature Erosion-Resistant Ceramic Coatings, *Proc. Coatings for Aerospace and Automotive Industries (CAAI-6),* October 20-22 (Toronto, Canada), 1999, p 14-15
18. S. Thiele, R.B. Heimann, L.-M. Berger, M. Herrmann, M. Nebelung, T. Schnick, B. Wielage, and P. Vuoristo, Microstructure and Properties of Thermally Sprayed Silicon Nitride-Based Coatings, *J. Therm. Spray Technol.,* 2002, **11**(2), p 218-225
19. L.-M. Berger, M. Herrmann, M. Nebelung, R.B. Heimann, and B. Wielage, Modifizierte Siliciumnitrid-Kompositpulver für thermische Beschichtungs- technologien und Verfahren zu ihrer Herstellung, Offenlegungsschrift DE 196 12 926 A 1, Deutsches Patentamt, 2 Oktober 1997, in German
20. L.-M. Berger, M. Herrmann, M. Nebelung, R.B. Heimann, and B. Wielage, Modified Composite Silicon Nitride Powders for Thermal Coatings and Process for their Production, U.S. Patent 6,110,853, Aug 23, 2000
21. J. Kitamura, S. Usuba, Y. Kakudate, H. Yokoi, K. Yamamoto, A. Tanaka, and S. Fujiwara, Boron Carbide Coating by EMAP Spraying, *J. Therm. Spray Technol.,* 2003, **12**(1), p 70-76
22. S. Usuba, J. Kitamura, and Y. Kakudate, Spray Deposition of Ceramics Powders by Pulsed High Current Arc Plasma, *Proc. 1st Tsukuba Intern. (Japanese-German) Coatings Symp.,* May 17, 2004 (Tsukuba, Japan), p 20-21
23. G. Petzow and M. Herrmann, Silicon Nitride Ceramics, *Structure and Bonding,* Vol 102, Springer, Berlin/Heidelberg, Germany, 2002, p 47-67
24. R.B. Heimann and J. Kleiman, Shock-Induced Growth of Superhard Materials, *Crystals, Growth, Properties, and Applications,* Vol 11, H.C. Freyhardt, Ed., Springer, Berlin/Heidelberg, Germany, 1988, p 5-11
25. R.B. Heimann, *Plasma-Spray Coating. Principles and Applications,* VCH Weinheim, New York/Basel, 1996, p 144-147
26. D. Beegan and M.T. Laugier, Application of Composite Hardness Models to Copper Thin Film Hardness Measurement, *Surf. Coat. Technol.,* 2005, **199,** p 32-37
27. H. Tomizawa and T.E. Fischer, Friction and Wear of Silicon Nitride and Silicon Carbide in Water: Hydrodynamic Lubrication at Low Sliding Speed Obtained by Tribochemical Wear, *ASLE Trans.,* 1987, **30**(1), p 41-46
28. N. Umehara and K. Kato, The Effect of Initial Surface Roughness on Friction of Self-Mating Silicon Nitride in Water", *J. Jap. Soc. Tribolog.,* 1994, **39**(7), p 879-885, in Japanese
29. M. Eriksson and S. Jacobson, Tribological Surfaces of Organic Brake Pads, *Tribol. Intern.,* 2000, **33**(12), p 817-827